

# The Finite-Amplitude Evolution of Mixed Kelvin–Rossby Wave Instability and Equatorial Superrotation in a Shallow-Water Model and an Idealized GCM

PABLO ZURITA-GOTOR

*Universidad Complutense de Madrid, and Instituto de Geociencia, Centro Mixto del Consejo Superior de Investigaciones Científicas, Madrid, Spain*

ISAAC M. HELD

*NOAA/Geophysical Fluid Dynamics Laboratory, Princeton, New Jersey*

(Manuscript received 16 December 2017, in final form 22 March 2018)

## ABSTRACT

An instability involving the resonant interaction of a Rossby wave and a Kelvin wave has been proposed to drive equatorial superrotation in planetary atmospheres with a substantially smaller radius or a smaller rotation rate than Earth, that is, with a large thermal Rossby number. To pursue this idea, this paper investigates the equilibration mechanism of Kelvin–Rossby instability by simulating the unforced initial-value problem in a shallow-water model and in a multilevel primitive equation model. Although the instability produces equatorward momentum fluxes in both models, only the multilevel model is found to superrotate. It is argued that the shortcoming of the shallow-water model is due to its difficulty in representing Kelvin wave breaking and dissipation, which is crucial for accelerating the flow in the tropics. In the absence of dissipation, the zonal momentum fluxed into the tropics is contained in the eddy contribution to the mass-weighted zonal wind rather than the zonal-mean zonal flow itself. In the shallow-water model, the zonal-mean zonal flow is only changed by the eddy potential vorticity flux, which is very small in our flow in the tropics and can only decelerate the flow in the absence of external vorticity stirring.


## 1. Introduction

A planetary atmosphere is said to superrotate when the wind at some location blows faster in the direction of rotation than the equatorial surface. This is invariably associated with prograde zonal winds over the equator, as inertial stability demands that atmospheric angular momentum decrease poleward on isentropic surfaces. Superrotation is not unusual in the solar system, being observed both in gas giants like Jupiter and Saturn and in small(er) planets and moons like Venus and Titan. It is not observed to any appreciable extent in present-day Earth's troposphere. Nevertheless, it is conceivable that Earth's atmosphere might transition to a strongly superrotating state if the tropics were to become more

active, for instance, in a warmer climate (Caballero and Huber 2010). The importance of understanding this transition is enhanced because there are suggestions that the dynamical feedbacks associated with increasing tropical upper-tropospheric westerlies could lead to abrupt climate change (Suarez and Duffy 1992; Saravanan 1993).

Because a symmetric circulation conserves angular momentum in the absence of dissipation, superrotation requires a momentum source at the equator (Hide 1969). In most geophysically relevant scenarios, this momentum source will be due to eddy stresses, so superrotation can be described as an example of an eddy-driven jet. The traditional paradigm for superrotation is based on the generation and propagation of Rossby waves, which decelerate the flow where they dissipate and drive a westerly acceleration over their source region (e.g., Vallis 2006). This would be analogous to the spinup of the extratropical eddy-driven jet except that other mechanisms than baroclinic instability must be responsible for generating the Rossby waves in the

---

 Denotes content that is immediately available upon publication as open access.

---

*Corresponding author:* Pablo Zurita-Gotor, pzurita@alum.mit.edu

DOI: 10.1175/JAS-D-17-0386.1

© 2018 American Meteorological Society. For information regarding reuse of this content and general copyright information, consult the [AMS Copyright Policy](https://www.ametsoc.org/PUBSReuseLicenses) ([www.ametsoc.org/PUBSReuseLicenses](https://www.ametsoc.org/PUBSReuseLicenses)).

tropics. A plausible forcing mechanism is localized tropical heating, either steady or transient. Idealized models subject to steady asymmetric thermal forcing in the tropics can produce superrotation (Suarez and Duffy 1992; Kraucunas and Hartmann 2005), while large-scale propagating convection like the terrestrial Madden-Julian oscillation may also play a role in convecting atmospheres (Lee 1999). Motivated by the superrotation of tidally locked planets, Showman and Polvani (2011) studied the atmospheric response to steady asymmetric heating in a hierarchy of atmospheric models. They noted important differences between divergent and nondivergent models and proposed an alternative superrotation mechanism based on the interaction between an equatorial Kelvin wave and an off-equatorial Rossby wave. The differential zonal propagation of these two waves gives rise to a meridional tilt in the geopotential height, which produces an equatorward eddy momentum flux. They argued that this mechanism could be more relevant for tropical eddy-driven jets than meridional Rossby wave propagation because Rossby wave forcing is weak at the equator (Sardeshmukh and Hoskins 1988) and tropical waves are often trapped meridionally (Matsuno 1966).

On the other hand, *spontaneous* transition to superrotation with no explicit tropical wave forcing (i.e., with zonally symmetric heating) has been found in some idealized model studies of nonconvecting atmospheres. For instance, Williams (2003) found that an idealized dry GCM produces superrotation when the subtropical (meaning thermally forced) jet is sufficiently close to the equator. Williams attributed this finding to the generation of Rossby waves by a form of barotropic instability, but it is difficult to reconcile the simulated behavior with traditional barotropic instability. More recently, Mitchell and Vallis (2010) and Potter et al. (2014) performed a systematic sensitivity analysis of the general circulation in the idealized Held and Suarez model (Held and Suarez 1994) to the model's external parameters. They found a robust transition to superrotation at large thermal Rossby numbers (i.e., for atmospheres with wide tropical regions), making this an appealing model for superrotation in small and/or slowly rotating planets and moons like Venus or Titan.

In the model of Potter et al. (2014), the waves transporting momentum into the equator are large scale (wavenumber 1) and equivalent barotropic and have a mixed meridional structure with Kelvin wave characteristics at the equator and Rossby wave characteristics in midlatitudes. This structure is similar to the forced solutions of Showman and Polvani (2011) for the Matsuno-Gill problem and can likewise produce equatorial acceleration based on the mechanism proposed

by these authors. The main difference is that the waves are now internally generated in the absence of asymmetric heating. A possible generation mechanism is an ageostrophic instability associated with the resonant interaction between a Kelvin wave and a Rossby wave that has been proposed by Iga and Matsuda (2005) to drive Venusian superrotation. Although coupled Kelvin-Rossby instabilities had been studied earlier in a number of contexts, such as the stability analysis of oceanic density currents (Sakai 1989; Gula et al. 2009) or the tropical atmosphere (Dunkerton 1990; Winter and Schmitz 1998), Iga and Matsuda (2005) noted the possibility of a planetary-scale atmospheric version of this phenomenon as being relevant for superrotation. These authors studied the linear stability of plausible Venusian wind profiles in a shallow-water model, finding an unstable mode with mixed Kelvin-Rossby structure that grows by fluxing momentum from midlatitudes to the equator. More recently, Wang and Mitchell (2014) have studied the linear stability of a primitive equation model for parameter regimes representative of the superrotating simulations of Potter et al. (2014), finding again coupled Kelvin-Rossby modes with equatorward momentum fluxes.

It is plausible that this ageostrophic barotropic instability may also be responsible for superrotation in the simulations of Williams (2003), as conventional barotropic instability cannot produce a westerly acceleration at the equator without a reversal in sign of the equatorial-mean vorticity gradient. Ageostrophic divergence adds a layer of complexity to classical quasi-geostrophic barotropic and baroclinic stability. Instability conditions are more difficult to assess (Ripa 1983) and do not constrain the flow as much as in the balanced case: a large number of modes combining balanced and unbalanced motions are typically found even if growth rates are small [even the simple Couette flow becomes unstable in that case—albeit weakly so as the Rossby number ( $Ro$ ) approaches zero—as noted by Vanneste and Yavneh (2007)]. Nevertheless, there are cases in which unstable modes can be most easily understood as involving the interaction between a Kelvin component and a Rossby component (e.g., Sakai 1989).

An additional argument for the relevance of Kelvin waves for shear instability coupling midlatitudes with the tropics can be made using pseudomomentum arguments. With the standard sign conventions, eddies with positive (negative) pseudomomentum propagate westward (eastward) relative to the mean flow and tend to accelerate the mean flow in that direction when they are dissipated. In addition, unstable modes must have zero pseudomomentum. As a result, one may interpret some unstable modes as the superposition (or resonance) of

neutral modes with different-sign pseudomomentum (Hayashi and Young 1987). Since Rossby waves have westerly pseudomomentum in a positive PV gradient, unstable resonance must necessarily involve interaction with a mode with easterly pseudomomentum, such as the Kelvin wave. There is thus an analogy between Kelvin–Rossby instability and classical barotropic Rossby–Rossby instability, with the equator playing the role of the region of negative PV gradient. The pseudomomentum conservation relation is

$$\frac{\partial A}{\partial t} + \nabla \cdot F = \text{Dissipation}, \tag{1}$$

where  $A$  is pseudomomentum and  $F$  the Eliassen–Palm (EP) flux (Andrews and McIntyre 1976). Growth of the instability requires an EP flux from the regions with easterly pseudomomentum to the regions with westerly pseudomomentum or a momentum flux in the opposite direction. Specifically, the precise forms of  $A$  and  $F$  for the shallow-water model are

$$A = \frac{\bar{h}^2}{2} \frac{\bar{q}^2}{\bar{q}_y} - \bar{u}'\bar{h}' \quad \text{and} \quad F = -\bar{h}'\bar{u}'\bar{v}', \tag{2}$$

where  $u$  and  $v$  are the horizontal wind components,  $h$  is height, and  $q$  is potential vorticity. Only the first (second) component of  $A$  is nonzero for a pure Rossby (Kelvin) component. As a result of these constraints, a growing Kelvin–Rossby mode must have an eddy momentum flux directed toward the equator as found by Iga and Matsuda (2005), who also interpret their results using pseudomomentum. When these modes dissipate, they drive an irreversible westerly (easterly) acceleration over the equator (midlatitudes).

As an intermediate step between the linear stability analysis of Wang and Mitchell (2014) and the superrotating forced-dissipative simulations of Potter et al. (2014), this paper investigates the equilibration of Kelvin–Rossby instability by simulating the unforced initial-value problem. Based on the arguments above, we would expect this equilibration to produce superrotation. We first study the equilibration in the shallow-water model, which is the simplest model that can capture the instability. No equatorial acceleration, in the sense of the generation of positive zonal-mean zonal wind, is found in this case, which is striking but nevertheless consistent with previous findings on shallow-water superrotation (Scott and Polvani 2008; Showman and Polvani 2010). Comparable simulations in a dry multilevel GCM are found to superrotate—explaining this difference is a major objective of our study.

The paper is structured as follows. Section 2 introduces the setup and the models used. Section 3 studies

the shallow-water equilibration, and section 4 describes the primitive equation simulations. We discuss the relation of our shallow-water results with previous studies in section 5, and section 6 concludes with a short summary.

## 2. Model setup

We will simulate the Kelvin–Rossby (KR) instability of a barotropic zonal jet  $\bar{u} \neq f(p)$  using both a one-layer model and a multilevel primitive equation model. Previous studies have shown that the parameter region of instability for these modes is narrow, requiring nonsmall Rossby numbers and Froude numbers of order 1. The former implies that the jet speed is not much smaller than  $\Omega a$ , which is more easily satisfied in small, slowly rotating planets. The latter stems from the requirement that the Kelvin and Rossby waves phase lock (or resonate), which only occurs for a limited parameter range.

Wang and Mitchell (2014) investigate the instability properties of a basic state consisting of a subtropical jet defined by angular momentum conservation  $\bar{u}(\phi) = \Omega a \sin(\phi) \tan(\phi)$  up to a latitude  $\phi_0$ , poleward of which the zonal wind tapers off as  $\exp(-\phi^2)$ . One problem with this choice of basic state is that it is associated in many cases with a reversal of the absolute vorticity gradient, which may lead to shortwave barotropic instability. To prevent this, we have chosen to define the basic state in terms of its absolute vorticity instead, as follows:

$$\xi_a = f + \xi = \begin{cases} \alpha f = 2\Omega\alpha \sin(\phi), & |\phi| \leq \phi_0 \\ \alpha_2 f = 2\Omega[\cos^{-2}(\phi_0) - \alpha \tan^2(\phi_0)]\sin(\phi), & |\phi| > \phi_0 \end{cases} \tag{3}$$

so that absolute vorticity is a constant fraction,  $\alpha$  or  $\alpha_2$ , of the Coriolis parameter on the equatorward and poleward sides of the jet, respectively. We will only consider cases with  $\alpha < 1$ , with the limit  $\alpha = 0$  corresponding to angular momentum conservation. In contrast, the constant  $\alpha_2$  will always exceed 1 because we define it with the condition that the area-weighted relative vorticity integrates globally to zero, which gives  $\alpha_2 = \cos^{-2}(\phi_0) - \alpha \tan^2(\phi_0)$ . This ensures that the zonal wind goes to zero at both the equator and the poles. In practice, we smooth the vorticity jump at  $\phi = \phi_0$  using a tanh function with  $\delta\phi = 5^\circ$  to reduce small-scale ripples in our spectral model.

Figures 1a and 1b show the absolute vorticity and zonal wind with  $\phi_0 = 50^\circ$  and  $\alpha = 0$  or  $\alpha = 0.4$  for a planet with the same rotational speed as Earth and a radius 4 times smaller (the configuration used in our

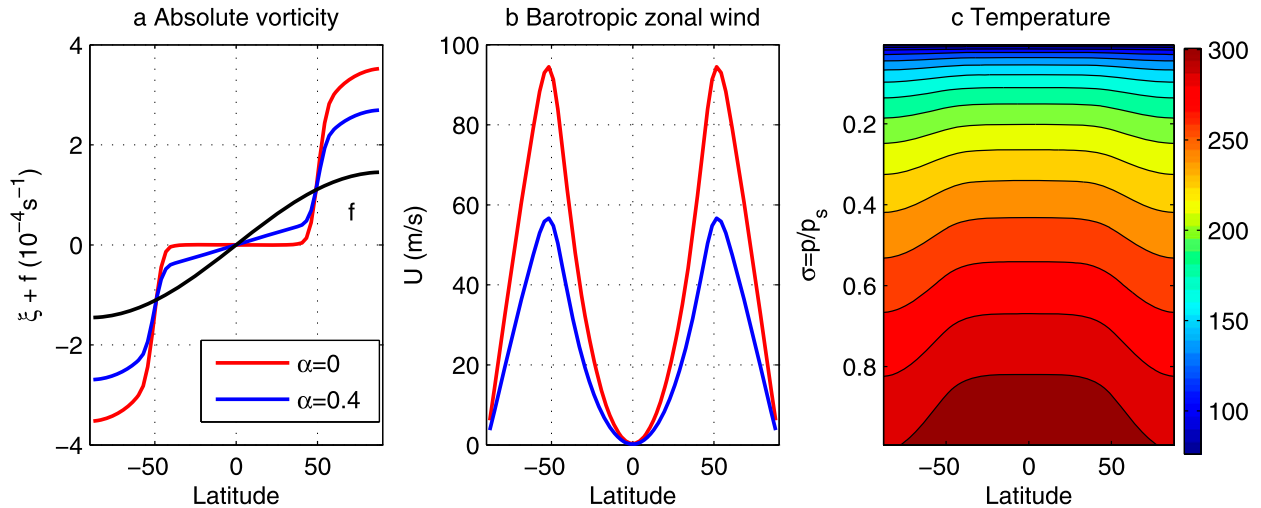


FIG. 1. (a) Absolute vorticity for the basic states with  $\alpha = 0$  (red) and  $\alpha = 0.4$  (blue) for a planet 4 times smaller than Earth. The Coriolis parameter is also shown in black for reference. (b) Zonal wind profiles for the same basic states. (c) Initial balanced temperature for the multilevel simulation with  $\alpha = 0$  and  $\Delta\Theta = 10$  K.

simulations). The main difference with the basic state of Wang and Mitchell (2014) is that relative vorticity does not go to zero at the pole, which is more consistent with the basic states of Iga and Matsuda (2005). This difference should have little impact on the KR modes on the equatorward side of the jet (our results with  $\alpha = 0$  are similar to those of Wang and Mitchell despite the different basic state).

To study the instability and equilibration of the above wind profile, it is necessary to construct an initial balanced state. There are two ways to achieve this in the shallow-water model (Iga and Matsuda 2005). One can start from a perturbed basic state  $\bar{h}_0(\phi)$  in nonlinear wind balance with the zonal wind profile:

$$f\bar{u}_0(\phi) + \frac{\bar{u}_0(\phi)^2 \tan(\phi)}{a} = -\frac{g}{a} \frac{\partial \bar{h}_0(\phi)}{\partial \phi}, \quad (4)$$

where bars indicate zonal means and  $\bar{u}_0(\phi)$  is the wind profile defined above. Alternatively, one can take  $\bar{h}_0(\phi) = H_0 = \text{constant}$  (where  $H_0$  is the mean fluid depth) and add a topographic forcing to the shallow-water  $y$ -momentum equation, which becomes

$$\frac{\partial v}{\partial t} + \frac{u}{a \cos(\phi)} \frac{\partial v}{\partial \lambda} + \frac{v}{a} \frac{\partial v}{\partial \phi} + \frac{u^2 \tan(\phi)}{a} + fu = -\frac{g}{a} \frac{\partial (h + h_T)}{\partial \phi},$$

with the topography defined by  $-g\partial h_T / a\partial\phi = f\bar{u}_0(\phi) + \bar{u}_0(\phi)^2 \tan(\phi)/a$ . In the narrow parameter regime of instability where the Kelvin and Rossby waves phase lock with Rossby numbers of order 1, we have  $c_K \sim O(\sqrt{gH_0}) \sim c_R \sim O(\Omega a)$ . This sets a constraint on

the mean fluid depth  $H_0$ , which must be on the order of the equator-to-pole height difference imposed by geostrophic balance [Eq. (4)]. We utilize the topography to prevent small or negative values of  $\bar{h}$  at the poles. Except for this zonal-mean topography, our shallow-water model is standard.

Constructing an initial state in balance with an arbitrary zonal wind profile in a primitive equation model is not trivial (e.g., Polvani and Esler 2007). However, things are much simpler with our barotropic basic state in which  $\bar{u}_0$  is independent of  $p$  and  $\bar{\theta}_0 = \Theta_R(p)$  is independent of  $y$ , where  $\Theta_R$  is a reference potential temperature profile (defined below). We first calculate the surface pressure field  $\bar{p}_{s0}$  in balance with the initial wind profile integrating the equation

$$f\bar{u}_0 + \frac{\bar{u}_0^2 \tan(\phi)}{a} = -\frac{1}{\rho_0 a} \frac{\partial \bar{p}_{s0}}{\partial \phi} = -R\Theta_R(\bar{p}_{s0}) \left(\frac{\bar{p}_{s0}}{p_0}\right)^\kappa \frac{\partial \log \bar{p}_{s0}}{a \partial \phi}. \quad (5)$$

After computing  $\bar{p}_{s0}$ , it is trivial to calculate the initial temperature field at the pressure/sigma levels in terms of the reference potential temperature profile  $\Theta_R(p)$ . This is shown in Fig. 1c for the basic state with  $\alpha = 0$  (the isotherms are not horizontal using a sigma vertical scale because of the large surface pressure changes).

To integrate Eq. (5), we need to provide a polar surface pressure. We use the value  $p_{s0}(-\pi/2) = 1000$  hPa, much larger than typical meridional pressure variations, to avoid the negative-depth problems found in the shallow-water model. This in practice prevents external Kelvin–Rossby instabilities—we will focus on instabilities due

to interaction between Rossby waves and internal, vertically propagating Kelvin waves. These are sensitive to the reference temperature profile, for which we choose a simple, uniformly stratified profile that extends to the top model level at 4.6 hPa (there is no tropopause):

$$\Theta_R(p) = \Theta_0 - \Delta\Theta \log\left(\frac{p}{p_0}\right). \quad (6)$$

This profile has stratification  $\partial\Theta_R/\partial z \approx \Delta\Theta/H$  ( $H$  is the density scale height) so that vertically propagating Kelvin waves with vertical wavelength  $L_z$  have zonal phase speed  $c_K \propto NL_z \sim \sqrt{gL_z^2\Delta\Theta/(\Theta_0H)}$ . We will use in this paper  $\Delta\Theta = 10\text{ K}$  and the reference values  $p_0 = 10^5\text{ Pa}$  and  $\Theta_0 = 300\text{ K}$ . Finally, we note that a sponge is added to damp the eddies near the model top with viscosity  $\nu(\sigma) = 10^7 \exp[-(\sigma/0.05)^2] (\text{m}^2\text{ s}^{-1})$ . We have performed a sensitivity analysis varying the depth and strength of the sponge to make sure that our results are robust.

We have chosen this barotropic state for the primitive equation model to avoid any possibility of baroclinic instability and to provide a cleaner comparison with the shallow-water model. The hope is that the characteristics of the evolution of this KR instability is qualitatively similar when it is isolated from baroclinic instability in this way and when it is competing with baroclinic instability in more realistic settings.

In the following sections, we describe the growth and equilibration of the KR modes in the two models. In both cases, the simulations are initialized adding a small perturbation to the balanced barotropic jet described above. This perturbation is small enough that the most unstable mode has time to emerge before the eddies become nonlinear (as manifest by the uniform exponential growth and robust wave-1 perturbation structure through a few decades of eddy kinetic energy; see, e.g., Fig. 2a). We do not emphasize the linear instability analysis itself as these are covered by Iga and Matsuda (2005) and Wang and Mitchell (2014) for the shallow-water and primitive equation instabilities, respectively.

### 3. Shallow-water results

We consider a basic state with a midlatitude jet defined by angular momentum conservation ( $\alpha = 0$ ) up to a latitude  $\phi_0 = 50^\circ$ , in a planet with the same rotation speed as Earth but a size 4 times smaller (thick red line in Fig. 1). A T42 resolution is sufficient for this small planet size, in which wavenumber 1 dominates. With the chosen configuration, the most unstable mode is obtained near the shallow-water depth  $gH_0 = 1000\text{ m}^2\text{ s}^{-2}$ .

Note that although the parameter regime of KR instability is narrow, this instability is not weak: the  $e$ -folding time is less than a day with these parameters ( $\sigma^{-1} \approx 0.75\text{ days}$ ).

Figure 2b shows the structure of the perturbation that emerges near the end of the linear growth stage (corresponding to the time  $t = 10\text{ days}$  in Fig. 2a). The unstable mode has the characteristic KR structure described in previous studies, coupling an equatorial Kelvin wave with a Rossby wave propagating on the midlatitude jet. Also consistent with previous studies, the mode has a robust equatorward momentum flux (Fig. 2c), which one is tempted to use as a smoking gun for superrotation. Yet the actual rate of change of the zonal-mean zonal wind vanishes over a broad tropical region (blue line in Fig. 2d).

We can understand the lack of equatorial acceleration by writing the zonal momentum equation in the form

$$\frac{\partial \bar{u}}{\partial t} = \overline{v(f + \xi)}. \quad (7)$$

Zonal-mean zonal wind acceleration requires a positive eddy vorticity flux. This can only happen in the presence of a tropical Rossby wave source, as Rossby wave growth or dissipation/breaking can only decelerate the flow with a positive vorticity gradient.

For the specific KR instability problem considered here, tropical vorticity fluxes are not just negative but also very small. The symmetry of the problem demands a zero-vorticity flux at the equator [the importance of which is emphasized in this context by Showman and Polvani (2011)], but the region of weak vorticity flux is broad and persists when symmetry is broken (not shown). It owes its existence to the smallness of absolute vorticity over a broad tropical region characteristic of KR instability. With weak vortex stretching, vorticity is approximately conserved, and the weak vorticity gradients then imply small vorticity fluxes. As shown in Fig. 2d, these fluxes vanish exactly in the zero-vorticity limit  $\alpha = 0$ .

To understand how the lack of tropical acceleration may be consistent with the equatorial convergence of the eddy (angular) momentum flux, we decompose this convergence as follows:

$$-\frac{1}{a \cos^2(\phi)} \frac{\partial \overline{u'v' \cos^2(\phi)}}{\partial \phi} = \overline{v'\xi'} - \overline{u'D'}, \quad (8)$$

where  $D = (a \cos\phi)^{-1}(\partial u/\partial \lambda + \partial v \cos\phi/\partial \phi)$  is the divergence. The first term on the rhs, the eddy vorticity flux, dominates the eddy momentum flux convergence in the extratropics but is very small in the tropics of our



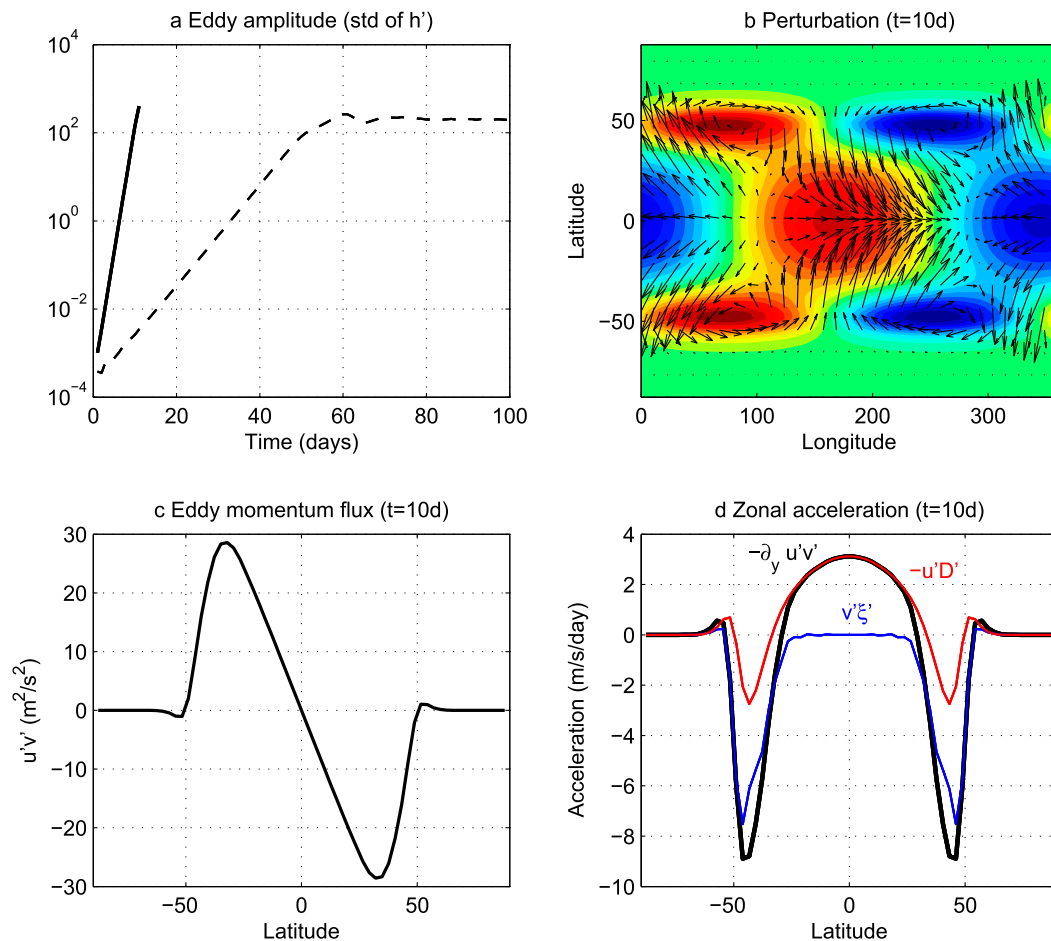


FIG. 2. (a) Time series of the domain-averaged standard deviation of the eddy height anomaly for the simulations with  $\alpha = 0$  (solid) and  $\alpha = 0.4$  (dashed); (b) anomaly structure at  $t = 10$  days with  $\alpha = 0$ : geopotential (shading) and velocity (vectors); (c) eddy momentum flux for the same simulation; and (d) zonal acceleration by the eddy momentum convergence (thick black) and its partition into the eddy vorticity flux (blue) and the divergent momentum convergence (red).

model, where the rotational flow is very weak. As a result (cf. Fig. 2d), the full eddy momentum convergence is dominated by the second term  $\overline{u'D'} < 0$ , the negative correlation between  $u'$  and  $D'$  arising from the longitudinal shift of the equatorial convergence eastward of the height maximum (Fig. 2c; see also Showman and Polvani 2011). This term is associated with meridional mass convergence (divergence) over longitudinal sectors with westerly (easterly) zonal flow, which increases the eddy component  $\overline{u'h'}$  of the mass-weighted momentum  $\overline{h\bar{u}^*} = \overline{h\bar{u}} + \overline{u'h'}$  at the equator. However, as discussed in appendix A [and made apparent by Eq. (7)], the change in the Eulerian-mean momentum  $\bar{u}$  can only be driven by the eddy vorticity flux in the shallow-water model.

It is not possible to continue the above simulation very far into the nonlinear regime without some

treatment of Kelvin wave breaking, which is violent in this single-layer model. As the simulation becomes nonlinear, the Kelvin wave steepens, creating a discontinuity in the height field and emitting abundant gravity wave radiation. The simulation breaks down as the height field eventually goes to zero somewhere in the domain. Numerically stable solutions are difficult to obtain, especially in the spectral model utilized here. Thus, we use a less unstable simulation with  $\alpha = 0.4$  (dashed line in Fig. 2a) to more easily study the equilibration of the instability.

Figures 3a–c show time series of the eddy vorticity flux (Fig. 3a), the total eddy momentum convergence (Fig. 3b), and the divergent contribution to this convergence  $-\overline{u'D'}$  (Fig. 3c) for this simulation. We can see that the eddy vorticity flux is still very small over a broad equatorial band for this value of  $\alpha$  (even though

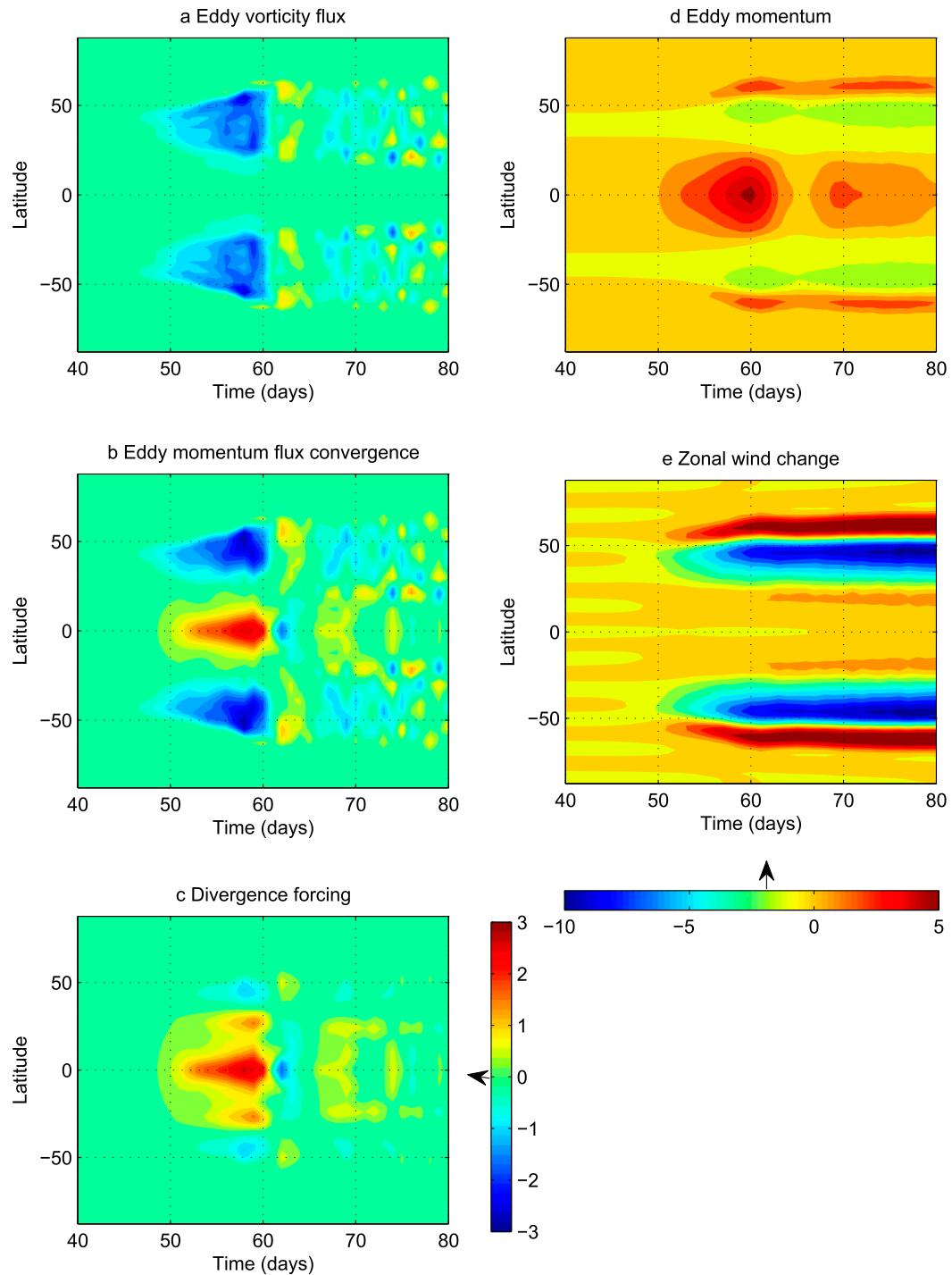


FIG. 3. For the simulation with  $\alpha = 0.4$ , (a)–(c) time series of zonal acceleration ( $m s^{-1} day^{-1}$ ) by (a) the eddy vorticity flux, (b) the eddy momentum flux convergence, and (c) the divergence forcing; all panels use the vertical color bar. (d) Eddy momentum  $\overline{u'h'/h}$  and (e) zonal wind change from the initial state; both panels use the horizontal color bar.

absolute vorticity no longer vanishes) so that the eddy momentum flux convergence is again strongly dominated by the divergent forcing. Consistent with this, the

increase in the mass-weighted momentum is entirely due to the eddy component  $\overline{u'h'}$ , (Fig. 3d) and there is no superrotation (Fig. 3e).

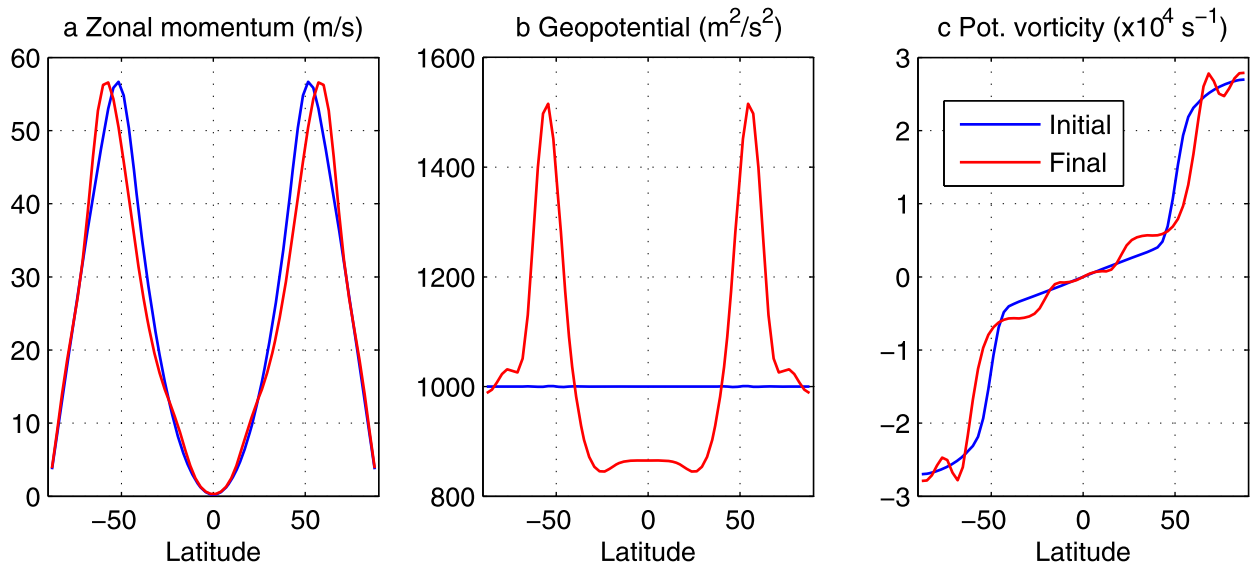


FIG. 4. Initial (blue) and final (red) meridional profiles of (a) zonal momentum, (b) geopotential  $gh$ , and (c) potential vorticity  $H_0 \bar{Q}$  for the simulation with  $\alpha = 0.4$ .

The equilibration of the instability is evidently controlled by the extratropical vorticity fluxes in the Rossby wave component. The most important effect is likely to be the generation of regions of well-mixed PV just equatorward of the jets (Fig. 4c; the jets move poleward slightly), which occurs near the unstable mode's steering latitude, where the interaction between Kelvin and Rossby wave components is presumably concentrated (Iga and Matsuda 2005). There is also a poleward shift of the midlatitude jets (Fig. 4a) and associated PV fronts (Fig. 4c). Over the tropics, a shallowing of the fluid depth by the total meridional mass flux, or residual circulation, decreases the phase speed of the equatorial Kelvin wave, which could also contribute to a reduction in phase locking.

The results in this section illustrate how the KR instability in this shallow-water model can grow and transport momentum equatorward without modifying the zonal-mean zonal flow significantly, consistent with the necessarily small vorticity flux in the tropics. Some mechanism for dissipating the Kelvin wave component of the KR instability is needed to produce westerly acceleration. Physically plausible Kelvin wave dissipation/breaking is far easier to achieve in a multilevel model with vertical propagation than in a shallow-water model, as illustrated in the following section.

#### 4. Multilevel results

Motivated by the failure of the shallow-water model to produce superrotation, we have studied the

equilibration of KR instability in the spectral primitive equation dynamical core described by Held and Suarez (1994), using again a T42 resolution and 80 vertical levels. We use the same barotropic wind profile of the previous section, with  $\alpha = 0$  and the surface pressure and temperature fields initialized as described in section 2. Fully replicating the shallow-water setup would require making the external Kelvin mode resonate with the extratropical Rossby wave, for which we would expect results similar to those of the previous section. Hence, we will focus instead on the instability arising from the resonant interaction between the Rossby wave and internal, vertically propagating Kelvin waves. Because our model has a sponge at the top (aiming to model a radiation boundary condition), these internal Kelvin waves are not free modes of the equations and would not exist in the absence of the extratropical Rossby wave. However, they can be maintained, forced by the instability, in spite of the upward radiation (we have varied the parameters of the sponge damping over a wide range to ensure the robustness of our results).

This is illustrated in Fig. 5c, which shows an equatorial cross section of the most unstable mode obtained using the control parameters ( $\Delta\Theta = 10$  K, which gives  $d\theta/dz \approx 1.2$  K km $^{-1}$  as discussed in section 2). For this stratification, the equivalent depth of the shallow-water most unstable mode ( $gh_e \approx 1000$  m $^2$  s $^{-2}$ ) is obtained with a vertical wavelength of about 31 km, which is in good agreement with the results of Fig. 5c (see also Fig. 6). The slightly weaker growth rate of this mode compared to the shallow-water model ( $\sigma^{-1} \approx 0.83$  days)



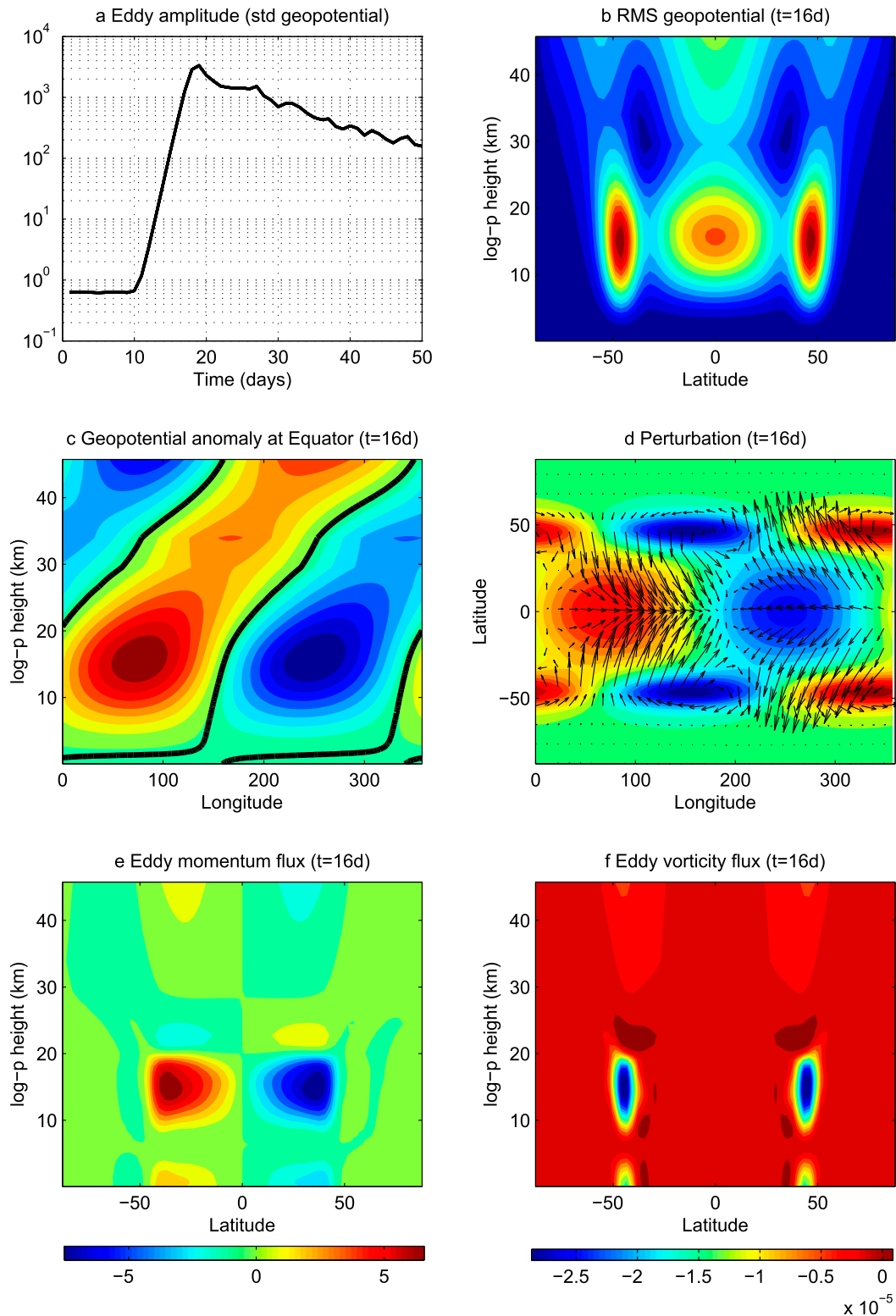


FIG. 5. For the multilevel model with  $\alpha = 0$ , (a) time series of domain-averaged eddy geopotential amplitude and (b)–(f) eddy structure at  $t = 16$  days: (b) zonal-mean eddy geopotential variance, (c) eddy geopotential at the equator, (d) anomaly structure at  $z = 15$  km for geopotential (shading) and velocity (vectors), (e) eddy momentum flux, and (f) eddy vorticity flux.

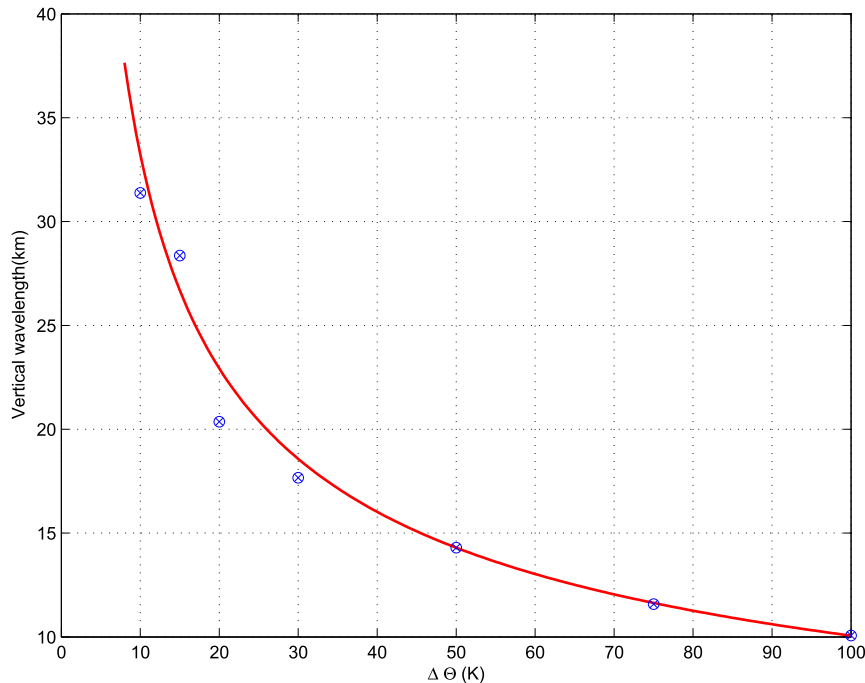


FIG. 6. Vertical wavelength in the primitive equation simulations as a function of the  $\Delta\Theta$  parameter. The red solid line shows the vertical wavelength that yields the equivalent depth  $gh_e = 1000 \text{ m}^2 \text{ s}^{-2}$  for the given stratification, calculated as  $2\pi/L_z = [N^2/(gh_e) - 1/(4H^2)]^{1/2}$ , where  $H$  is the scale height.

might be due to the energy leakage at the top. A more important difference is that while the shallow-water model has a narrow parameter regime of instability about the most unstable depth  $gH_0 \approx 1000 \text{ m}^2 \text{ s}^{-2}$ , the primitive equation model has a much broader instability range (in  $\Delta\Theta$  space) because the Kelvin waves are now able to choose their vertical scale to resonate with the Rossby wave. As  $\Delta\Theta$  increases, the vertical wavelength shrinks to keep the equivalent depth roughly constant at its optimal value (Fig. 6), with additional phases appearing in the vertical structure for the largest values of  $\Delta\Theta$  (not shown). We emphasize that this vertical wavelength changes continuously and is not quantized, as all these Kelvin waves propagate vertically. The growth rate is roughly the same for all these simulations (not shown).

A more detailed description of the spatial structure of the anomaly with the control parameters after 16 days (by which time the most unstable mode has emerged; see Fig. 5a) is provided in other panels of Fig. 5. Figure 5b shows that the mode reaches its peak amplitudes at the latitude of the jet and at the equator. The horizontal structure at the wave maximum ( $z \approx 15 \text{ km}$ ) is reminiscent of that found in the shallow-water case (Fig. 5d). Finally, the eddy momentum and vorticity fluxes (Figs. 5e,f) also have similar meridional structures to

their shallow-water counterparts: there are robust equatorward momentum fluxes in both hemispheres but very weak eddy vorticity fluxes over the whole tropics.

In contrast with the shallow-water model, these equatorward momentum fluxes are now able to induce robust superrotation (Fig. 7a). For one perspective on this difference, it is useful to consider the zonal-mean zonal momentum equation in isentropic coordinates (homomorphic with the shallow-water equations), using again its vector invariant form:

$$\frac{\partial \bar{u}_\theta}{\partial t} = \overline{v_\theta (f + \xi_\theta)} - \overline{\dot{Q} \frac{\partial u_\theta}{\partial \theta}}, \quad (9)$$

where  $\dot{Q}$  is the heating rate and the  $\theta$  subscript indicates that all horizontal derivatives and velocities are calculated along isentropic surfaces. As in the previous case, eddy vorticity mixing (Rossby wave breaking) provides a mechanism to accelerate the flow, but this would require a Rossby wave source at the equator, and we expect the isentropic vorticity fluxes to be small like the isobaric fluxes in Fig. 5f. However, this is no longer the only route to superrotation as the mean flow can now also be accelerated by cross-isentropic advection (second term on the right-hand side). Although our model is formally adiabatic, we show below that the breaking and

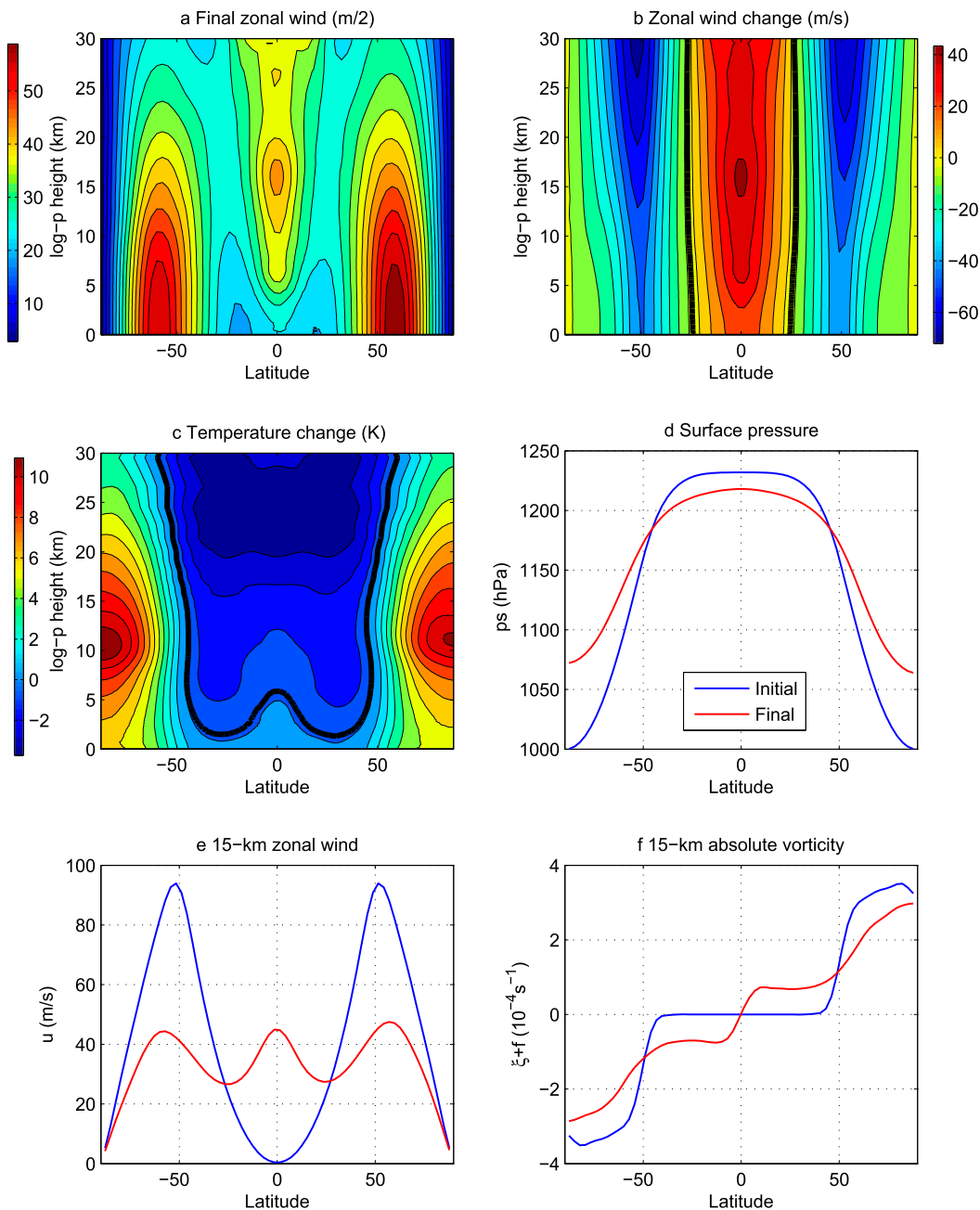


FIG. 7. Final state of the control run ( $\alpha=0$ ): (a) zonal wind; (b) zonal wind change from initial state; (c) temperature change from initial state; (d) initial (blue) and final (red) surface pressure; (e) as in (d), but for zonal wind at  $z = 15$  km; and (f) as in (d), but for absolute vorticity.

dissipation of the Kelvin wave gives rise to cross-isentropic mixing.

Physically, we can understand this result as a consequence of Kelvin’s circulation theorem. As a material contour is deformed by the eddies, any Eulerian-mean acceleration is reversible up to the point when dissipation occurs—the circulation along the contour remains

unchanged until dissipation gives rise to irreversible mass transport across the contour and induces a net acceleration. For vorticity waves, this dissipation occurs as Rossby wave breaking induces a mass transport across vorticity contours on isentropic surfaces. In contrast, Kelvin wave dissipation is associated with irreversible mass transport across isentropic contours,

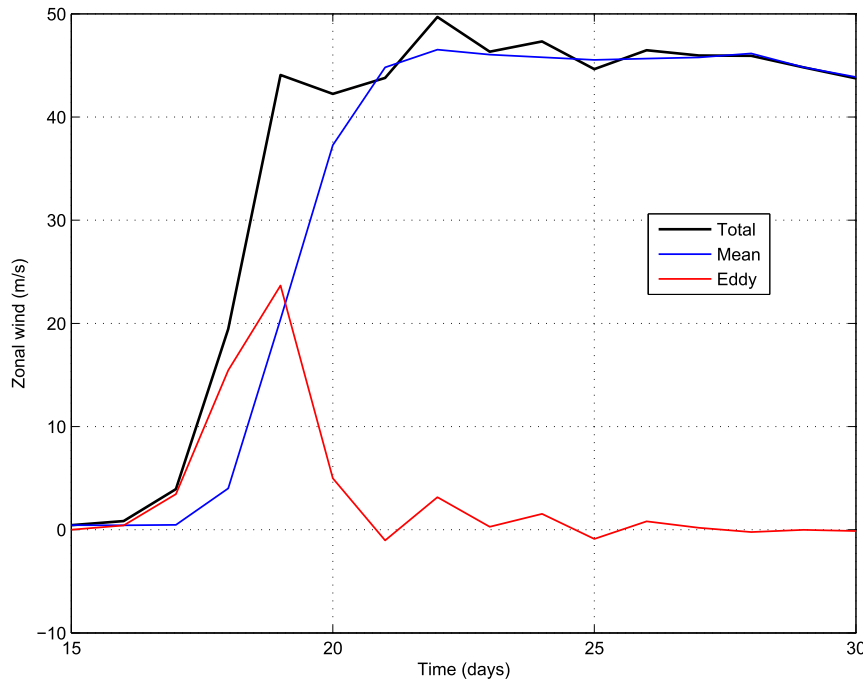


FIG. 8. Time series of Eulerian-mean momentum  $\bar{u}$  (blue), eddy momentum  $\overline{u'h'/h}$  (red), and net mass-weighted momentum  $\bar{u}^*$  (black) in isentropic coordinates for the primitive equation model at the equator at the 315-K isentropic level.

approximately in the vertical direction. Failure of our shallow-water model to superrotate can then be attributed to its inability to produce the required Kelvin wave breaking and dissipation in this direction.

To test these ideas, we have performed an isentropic analysis of our control primitive equation simulation. Figure 8 shows time series of the Eulerian-mean wind  $\bar{u}$ , the eddy component  $\overline{u'h'/h}$ , and the total mass-weighted wind  $\bar{u}^*$  in isentropic coordinates ( $h$  is the isentropic thickness in this context), averaged near the level of maximum acceleration (315 K). We can see that in the early phases of the equilibration (days 17–18), only  $\overline{u'h'}$  increases while  $\bar{u}$  remains unchanged, similar to the shallow-water results. We may think of this as a quasi-linear stage, during which eddies grow to finite amplitude but do not break. However, after a short delay, the instability is able to modify  $\bar{u}$ , and by the end of the simulation, the response is dominated by the mean wind changes.

Figure 9 describes this process in more detail by showing the evolution of equatorial potential temperature between days 17 and 21 of the simulation. A wavy perturbation superimposed to the uniformly stratified profile is apparent at time  $t = 17$  days, near the end of the quasi-linear stage. At  $t = 18$  days, a strong thermal front is created around  $z = 15$  km as the Kelvin wave steepens. Small-scale structure is already apparent at this stage and intensifies notably by day  $t = 19$  days, including

regions with unstable stratification. Numerical dissipation must induce cross-isentropic transport at this stage, which leads to the dissipation of the thermal front a few days later ( $t = 21$  days; Fig. 9d). The dissipation of the front produces a negative  $\overline{Q\partial u_\theta/\partial\theta}$  and a mean-flow acceleration [cf. Eq. (9)] because the homogenization of isentropic thickness demands cross-isentropic transport from weakly to strongly stratified regions (high and low  $h'$ , respectively). These also correspond to regions with positive and negative  $u'$  because of the positive  $u'h'$  correlation so that the wave breaking essentially provides a mechanism to convert the eddy momentum  $\overline{u'h'}$  into a Eulerian-mean acceleration.

We have not attempted to document the dynamics of the Kelvin wave breaking in detail, which may involve small-scale frontal instability and gravity wave emission (e.g., Fritts et al. 1994), as the details of the breaking are likely sensitive to the numerics and not well resolved in our model. Our model is hydrostatic and has no convective adjustment or momentum transport so that convection only occurs on the (coarse) grid scale. A much higher resolution would also be needed to resolve the strong gravity wave radiation emitted during the breaking process. Our claim is that the zonal-mean momentum evolution is controlled to lowest order by the outer scale of the overturning Kelvin wave, the depth of the overturning region, and not by the details of

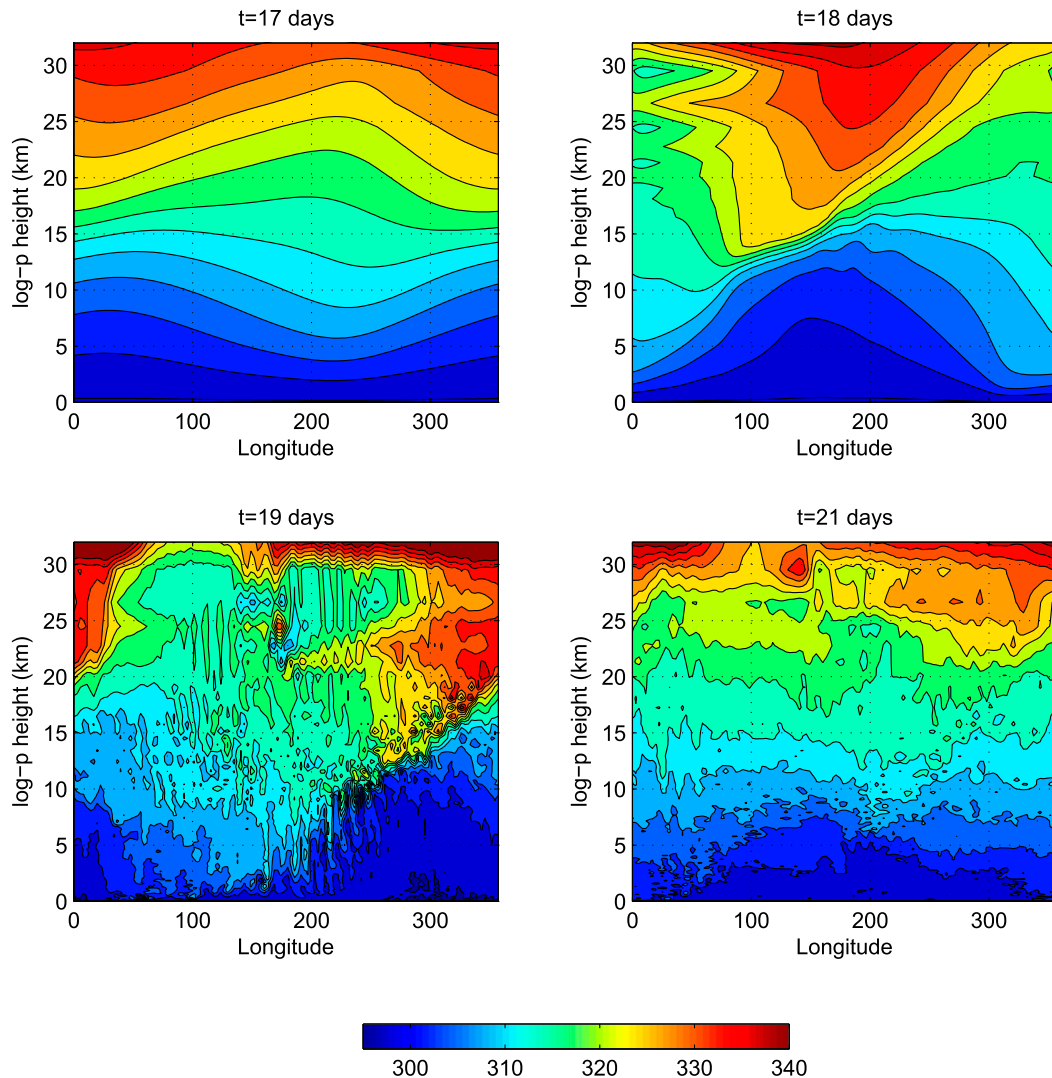


FIG. 9. Potential temperature on the equatorial plane from day 17 to day 21 of the simulation.

the wave breaking process. From the point of view of the large-scale circulation, the main reading of Fig. 9 is that the steepening of the Kelvin wave as the KR instability reaches finite amplitude and subsequent Kelvin wave breaking leads to dissipation and cross-isentropic mass transport in the primitive equation model. This cross-isentropic transport is likely crucial for allowing our model to equilibrate. Had we performed an actual adiabatic isentropic simulation, we would expect the simulation to break down as isentropic depth vanishes in some regions, similar to what we found in the shallow-water model. Presumably, the weakly unstable shallow-water simulation described in section 3 is able to equilibrate quasi linearly because  $\overline{u'h'}$  can reach its saturation level with  $h' < \bar{h}$  (cf., Fig. 3e) and Kelvin waves do not break.

Figure 10 describes the evolution of the main terms in the vertically averaged momentum balance during the equilibration of the KR instability, which produces a westerly acceleration at the equator (Fig. 10a). Since it is not straightforward to compute the cross-isentropic mixing from the model output, we use an indirect method to estimate this term. As shown in appendix B, we may approximate in the tropics for this problem:

$$\left\langle \dot{Q} \frac{\partial u_\theta}{\partial \theta} \right\rangle_\theta \approx \left\langle \omega \frac{\partial u}{\partial p} \right\rangle_p, \tag{10}$$

using angle brackets to denote mass-weighted vertical integrals in  $\theta$  or  $p$  coordinates. Thus, we estimate the net column acceleration by cross-isentropic mixing using the vertically integrated vertical advection in pressure

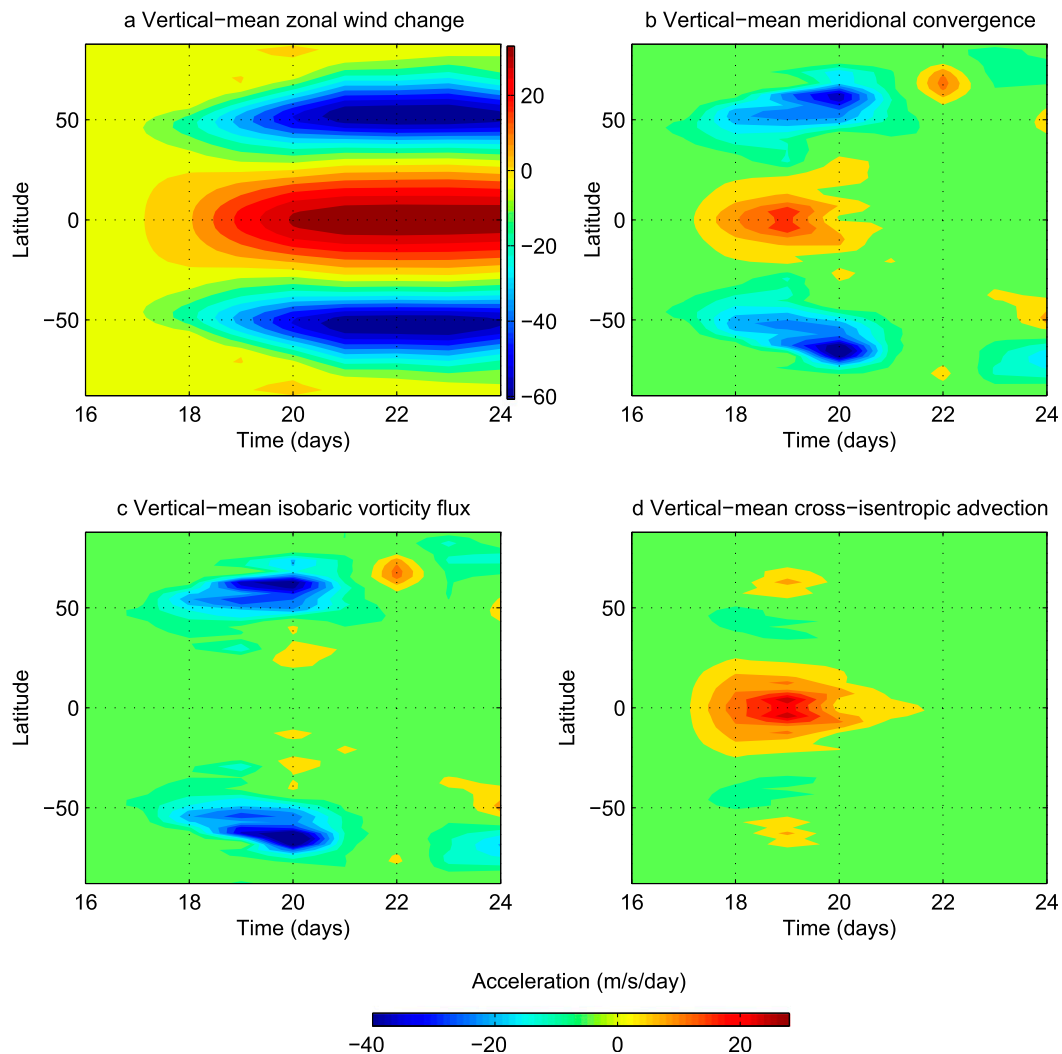


FIG. 10. For the control multilevel simulation ( $\alpha = 0$ ), time series of (a) vertically averaged zonal wind changes from the initial state, (b) vertically averaged eddy momentum flux convergence, (c) vertically averaged isobaric vorticity flux, and (d) vertically averaged cross-isentropic advection.

coordinates. Based on the divergence form of the momentum equation, the vertically averaged acceleration in Fig. 10a is forced by the vertically averaged meridional eddy momentum convergence associated with the instability (Fig. 10b). Using the vector invariant form, the eddy vorticity flux (Fig. 10c; here computed in isobaric coordinates) plays virtually no role, and the acceleration is entirely driven by the cross-isentropic mixing (Fig. 10d).

Figure 7 summarizes the mean flow adjustment for our  $\alpha = 0$  run with the full GCM. The equatorial acceleration (Figs. 7a,b) appears to be a key ingredient to the equilibration: once the equatorial westerlies develop, the Kelvin and Rossby waves are no longer able to phase lock in their counterpropagation, and the instability must necessarily shut down [this is why KR instability

may only spin up—but not maintain—equatorial superrotation, as noted by Pinto and Mitchell (2014)]. Although there is a poleward shift of the midlatitude jets as in the shallow-water case, this is now also accompanied by strong deceleration. We observe weak cooling (heating) over the tropical (extratropical) region (Fig. 7c) and a net poleward mass transport by the circulation (Fig. 7d). Figures 7e,f show the final wind and vorticity structure at the  $z = 15$ -km level. We can see that vorticity is efficiently mixed on both sides of the superrotating jet, with large vorticity gradient developing at the equator in association with that jet. This mixing on the sides of the jet presumably also helps to reduce the ability of the Rossby and Kelvin components of the instability to interact.



## 5. Comparison with other shallow-water simulations

There are obvious similarities between the results described here and superrotation in the forced simulations of [Showman and Polvani \(2011\)](#). In both cases, superrotation is driven by the interaction between a Kelvin wave and a Rossby wave, though the forcing mechanism for these waves is different. In the model of [Showman and Polvani \(2011\)](#), the waves are forced by asymmetric tropical heating as in [Gill \(1980\)](#), while in our model, they are generated spontaneously by an ageostrophic instability.

[Showman and Polvani \(2011\)](#) find superrotation in both shallow-water and primitive equation simulations but *only when vertical momentum advection is included* in the former. The issue is discussed in more detail by [Showman and Polvani \(2010\)](#). Using a standard one-layer model forced by mass sources and sinks, these authors find eddy momentum convergence but no mean-flow acceleration at the equator, as the equatorial momentum convergence is cancelled by  $u'D'$  in their Eulerian-mean zonal wind balance [cf. their Eq. (5) and Fig. 1c]. This implies that the eddy vorticity flux vanishes and all the eddy momentum convergence is due to the divergent motions as in our simulations. Interestingly, [Showman and Polvani](#) were able to achieve superrotation when vertical (cross isentropic) momentum advection was included in their model, mimicking the exchange of momentum with a motionless lower layer accompanying mass exchange, using the “first-order upstream” formulation of [Shell and Held \[2004\]](#); this is the setup used in the more comprehensive simulations of [Showman and Polvani \(2011\)](#). This momentum exchange can be effective in damping forced Kelvin wave–like circulations.

Motivated by these results for a forced problem, we tried adding nonconservative terms to our unforced shallow-water model. Adding simple linear thermal (height) damping to our shallow-water model, we could only achieve weak equatorial westerlies even when including the momentum transport associated with the implied mass transport. This weakness in our case is likely connected to the fact that increasing the damping to dissipate the Kelvin wave more efficiently is presumably also enough to stabilize the flow. We also attempted nonlinear damping or, as an alternative, a simple mass adjustment scheme in the shallow-water model that injected mass into the layer whenever its depth went below some small, specified threshold. We were able to obtain shallow-water superrotation with this method, although in the more unstable simulations, the mean depth increased by a large factor, a behavior not seen in our multilevel results.

The difficulty of forcing shallow-water superrotation in a Gill-like setting, with imposed asymmetric tropical heating, and its sensitivity to nonconservative effects, can be contrasted to the case studied by [Suhas et al. \(2017\)](#) in which Rossby wave propagation can drive shallow-water superrotation when the vorticity equation is forced directly (as opposed to forcing the continuity/thermodynamic equation). The latter is consistent with the standard paradigm of superrotation forced by Rossby wave propagation out of the tropics (e.g., [Suarez and Duffy 1992](#)) but does not address the physical plausibility of vorticity stirring versus thermal forcing (or mass sources/sinks) in the shallow-water context.

In our study, the generation of the wave is spontaneous, being an instability that evolves from infinitesimal noise, so the question of sensitivity to the mode of forcing does not arise. However, we cannot avoid the question of the role of dissipation in the finite-amplitude evolution of the instability. Mixing of PV by the Rossby wave component of the instability in the subtropics and midlatitudes is present in all cases, but our results indicate that dissipation/breaking of the Kelvin wave component is essential for superrotation and difficult to mimic in a single-layer shallow-water context.

## 6. Concluding remarks

We have shown that a Kelvin–Rossby (KR) instability spins up an equatorial westerly jet as it equilibrates in an idealized GCM, supporting the notion that this instability is responsible for the superrotation in small/slowly rotating planets ([Iga and Matsuda 2005](#)) and in documented simulations with idealized GCMs at large thermal Rossby numbers ([Mitchell and Vallis 2010](#); [Potter et al. 2014](#)). The conditions for this are similar in kind to those required by other such instabilities: similar phase speeds of the Kelvin wave and Rossby wave components and spatial overlap between the two components. The latter is facilitated in small or slowly rotating planets and also provides a natural explanation for the results of [Williams \(2003\)](#) in which superrotation can be generated in an Earth-like GCM by moving the baroclinic zone closer to the equator.

The instabilities have the same qualitative structure in the shallow-water and multilevel simulations, with equatorward flux of angular momentum consistent with the form of the pseudomomentum. An interesting distinction is that, because the coupling in the multilevel case is between Rossby waves with maximum amplitude near the tropopause and vertically propagating

equatorial Kelvin waves, the instability is more robust in this case than in a shallow-water model because the vertical wavelength of the Kelvin wave can adjust so that its eastward phase speed matches that of the Rossby wave.

We find that conservative shallow-water simulations of the instability do not superrotate as measured by the zonal-mean zonal winds, as could be anticipated from the zonal-mean momentum equation. Some superrotation can be obtained when adding thermal or mechanical damping, but it is typically weak. A model with more vertical structure is needed to produce the superrotating state in a more robust manner. Our results underscore the important role played by breaking and dissipation of the Kelvin wave component of the instability, without which there can be no tropical acceleration in this model (Andrews and McIntyre 1976). While there is net equatorward momentum flux by this instability in both the shallow-water and multilevel GCM simulations, in the former, this momentum resides in the  $u'h'$  component, which is realized as a change in the zonal-mean zonal wind only when the Kelvin wave breaks.

Our simulations admittedly do not provide a clean simulation of the breaking process itself, which would likely require a different modeling strategy. For the purpose of this paper, we have tried to stay in the framework of a dynamical core study that is easily replicated without a full GCM and even without a subgrid vertical mixing scheme. Our hypothesis is that the details of the breaking do not affect the robustness of the generation of the superrotating state, which is controlled by the large-scale parameters of the breaking Kelvin wave.

We believe that this KR instability will prove to be a robust and centrally important component of planetary atmospheres with  $O(1)$  thermal Rossby numbers. Whether this coupled wave instability mechanism also operates in moist atmospheres in the terrestrial regime, especially as the atmosphere warms, with the slowing of eastward wave propagation through convective coupling allowing the KR instability to form with smaller thermal Rossby numbers, is clearly an important question for future work.

*Acknowledgments.* We are grateful to Adam Showman for clarifying to us the acceleration mechanism in his forced simulations, as well as for several insightful comments. P. Z.-G. acknowledges financial support by Grant CGL2015-72259-EXP by the Ministry of Economy and Competitiveness of Spain. This work has been partly done during P. Z.-G.'s visit to Princeton, funded by NSF Grant AGS-1733818.

## APPENDIX A

### Forcing of the Eulerian-Mean Momentum in Layer Models

Consider an inviscid shallow-water model that conserves potential vorticity  $q = (f + \xi)/h$ , using Cartesian coordinates for simplicity. The transformed Eulerian-mean momentum equation for this model is

$$\frac{\partial \bar{u}}{\partial t} = (f + \bar{\xi})\bar{v} + \overline{v'\xi'} = (f + \bar{\xi})\bar{v}^* + \overline{h'v'q'}, \quad (\text{A1})$$

where  $\bar{v}^* = \bar{v} + \overline{v'h'/h}$  is the residual flow and the linearized eddy potential vorticity flux is

$$\overline{h'v'q'} = \overline{v'\xi'} - (f + \bar{\xi})\overline{v'h'/h}.$$

Combining Eq. (A1) with continuity,

$$\frac{\partial \bar{h}}{\partial t} = -\frac{\partial}{\partial y}(\bar{h}\bar{v}^*),$$

we obtain for the rate of change of the Eulerian-mean momentum,

$$\frac{\partial}{\partial t}(\bar{M}\bar{h}) = -\frac{\partial}{\partial y}(\bar{h}\bar{v}^*\bar{M}) + \overline{h^2v'q'}, \quad (\text{A2})$$

where  $M = u - \int f dy$  is absolute angular momentum.

On the other hand, we can combine the linearized eddy momentum and continuity equations (written for simplicity in a reference system moving with the mean flow):

$$\begin{aligned} \frac{\partial u'}{\partial t} &= (f + \bar{\xi})v' - g\frac{\partial h'}{\partial x}, \\ \frac{\partial h'}{\partial t} &= -v'\frac{\partial \bar{h}}{\partial y} - \bar{h}\frac{\partial v'}{\partial y} \end{aligned}$$

to obtain for the eddy component of the mass-weighted momentum,

$$\frac{\partial}{\partial t}(\overline{u'h'}) = -\overline{h^2v'q'} - \frac{\partial}{\partial y}(\bar{h}\overline{u'v'}). \quad (\text{A3})$$

Combining this equation with the tendency for the mean momentum equation [Eq. (A2)], we finally obtain for the mass-weighted momentum,

$$\frac{\partial}{\partial t}(\bar{h}\bar{M}^*) = -\frac{\partial}{\partial y}(\bar{h}\bar{v}^*\bar{M}) - \frac{\partial}{\partial y}(\bar{h}\overline{u'v'}). \quad (\text{A4})$$

Thus, we can see that the mass-weighted momentum  $\bar{h}\bar{M}^*$  is forced by the eddy momentum convergence  $-\partial(\bar{h}\overline{u'v'})/\partial y$  [which is also (minus) the pseudomomentum forcing for this model; e.g., Held (1985)], but

changing the Eulerian-mean momentum  $\overline{h\overline{M}}$  requires a nonzero PV flux [Eq. (A2)]. When the eddy PV flux is zero, as in the problem discussed in section 3 (in that problem,  $\overline{h'v'q'} \approx v'\xi'$  because  $f + \xi \approx 0$ ), the eddy momentum convergence only accelerates the eddy term  $u'h'$  [Eq. (A3)].

These arguments can be generalized to the continuous case replacing  $h$  with isentropic density in isentropic coordinates. A key difference in that case is the addition of a cross-isentropic advection term to the right-hand side of Eq. (A1), which can also accelerate the mean flow in the absence of an eddy PV flux. As shown in section 4, this is the dominant mechanism in the tropics of our primitive equation model.

APPENDIX B

Justification of the Approximation in Eq. (10)

In section 4, we use the vertically integrated vertical momentum advection in pressure coordinates as an estimate of the net cross-isentropic momentum mixing along the column. To justify this approximation, we first relate the angular momentum forcing in divergence form to the vorticity flux in pressure coordinates:

$$\frac{\partial}{\partial p}(\overline{\omega u}) + \frac{1}{a \cos^2 \phi} \frac{\partial}{\partial \phi}(\overline{vu \cos^2 \phi}) = \overline{\omega \frac{\partial u}{\partial p}} - \overline{v\xi}. \tag{B1}$$

Doing the same in isentropic coordinates,

$$\frac{\partial}{\partial \theta}(\overline{\sigma Q u_\theta}) + \frac{1}{a \cos^2 \phi} \frac{\partial}{\partial \phi}(\overline{\sigma v_\theta u_\theta \cos^2 \phi}) = \overline{\sigma Q \frac{\partial u_\theta}{\partial \theta}} - \overline{\sigma v_\theta \xi_\theta}, \tag{B2}$$

where  $\sigma = -\partial p / \partial \theta$  is isentropic density multiplied by gravity.

Since the left-hand sides of Eqs. (B1) and (B2) have the same vertical integral, equal to the net momentum convergence along the column, we obtain

$$\left\langle \overline{Q \frac{\partial u_\theta}{\partial \theta}} \right\rangle_\theta - \left\langle \overline{\omega \frac{\partial u}{\partial p}} \right\rangle_p = \left\langle \overline{v_\theta \xi_\theta} \right\rangle_\theta - \left\langle \overline{v\xi} \right\rangle_p, \tag{B3}$$

where angle brackets indicate mass-weighted vertical integrals in  $\theta$  or  $p$  coordinates. Because vorticity fluxes are very small in the tropics for this problem (both in  $\theta$  and  $p$  coordinates), the two terms on the left-hand side are very similar.

REFERENCES

Andrews, D., and M. E. McIntyre, 1976: Planetary waves in horizontal and vertical shear: The generalized Eliassen-Palm relation and the mean zonal acceleration. *J. Atmos. Sci.*, **33**,

2031–2048, [https://doi.org/10.1175/1520-0469\(1976\)033<2031:PWIHAV>2.0.CO;2](https://doi.org/10.1175/1520-0469(1976)033<2031:PWIHAV>2.0.CO;2).

Caballero, R., and M. Huber, 2010: Spontaneous transition to superrotation in warm climates simulated by CAM3. *Geophys. Res. Lett.*, **37**, L11701, <https://doi.org/10.1029/2010GL043468>.

Dias Pinto, J. R., and J. L. Mitchell, 2014: Atmospheric superrotation in an idealized GCM: Parameter dependence of the eddy response. *Icarus*, **238**, 93–109, <https://doi.org/10.1016/j.icarus.2014.04.036>.

Dunkerton, T. J., 1990: Eigenfrequencies and horizontal structure of divergent barotropic instability originating in tropical latitudes. *J. Atmos. Sci.*, **47**, 1288–1301, [https://doi.org/10.1175/1520-0469\(1990\)047<1288:EAHSOD>2.0.CO;2](https://doi.org/10.1175/1520-0469(1990)047<1288:EAHSOD>2.0.CO;2).

Fritts, D. C., J. R. Isler, and Ø. Andreassen, 1994: Gravity wave breaking in two and three dimensions: 2. Three-dimensional evolution and instability structure. *J. Geophys. Res.*, **99**, 8109–8123, <https://doi.org/10.1029/93JD03436>.

Gill, A., 1980: Some simple solutions for heat-induced tropical circulation. *Quart. J. Roy. Meteor. Soc.*, **106**, 447–462, <https://doi.org/10.1002/qj.49710644905>.

Gula, J., R. Plougonven, and V. Zeitlin, 2009: Ageostrophic instabilities of fronts in a channel in a stratified rotating fluid. *J. Fluid Mech.*, **627**, 485–507, <https://doi.org/10.1017/S0022112009006508>.

Hayashi, Y.-Y., and W. Young, 1987: Stable and unstable shear modes of rotating parallel flows in shallow water. *J. Fluid Mech.*, **184**, 477–504, <https://doi.org/10.1017/S0022112087002982>.

Held, I. M., 1985: Pseudomomentum and the orthogonality of modes in shear flows. *J. Atmos. Sci.*, **42**, 2280–2288, [https://doi.org/10.1175/1520-0469\(1985\)042<2280:PATOOM>2.0.CO;2](https://doi.org/10.1175/1520-0469(1985)042<2280:PATOOM>2.0.CO;2).

—, and M. J. Suarez, 1994: A proposal for the intercomparison of the dynamical cores of atmospheric general circulation models. *Bull. Amer. Meteor. Soc.*, **75**, 1825–1830, [https://doi.org/10.1175/1520-0477\(1994\)075<1825:APFTIO>2.0.CO;2](https://doi.org/10.1175/1520-0477(1994)075<1825:APFTIO>2.0.CO;2).

Hide, R., 1969: Dynamics of the atmospheres of the major planets with an appendix on the viscous boundary layer at the rigid bounding surface of an electrically-conducting rotating fluid in the presence of a magnetic field. *J. Atmos. Sci.*, **26**, 841–853, [https://doi.org/10.1175/1520-0469\(1969\)026<0841:DOTAOT>2.0.CO;2](https://doi.org/10.1175/1520-0469(1969)026<0841:DOTAOT>2.0.CO;2).

Iga, S.-i., and Y. Matsuda, 2005: Shear instability in a shallow water model with implications for the Venus atmosphere. *J. Atmos. Sci.*, **62**, 2514–2527, <https://doi.org/10.1175/JAS3484.1>.

Kraucunas, I., and D. L. Hartmann, 2005: Equatorial superrotation and the factors controlling the zonal-mean zonal winds in the tropical upper troposphere. *J. Atmos. Sci.*, **62**, 371–389, <https://doi.org/10.1175/JAS-3365.1>.

Lee, S., 1999: Why are the climatological zonal winds easterly in the equatorial upper troposphere? *J. Atmos. Sci.*, **56**, 1353–1363, [https://doi.org/10.1175/1520-0469\(1999\)056<1353:WATCZW>2.0.CO;2](https://doi.org/10.1175/1520-0469(1999)056<1353:WATCZW>2.0.CO;2).

Matsuno, T., 1966: Quasi-geostrophic motions in the equatorial area. *J. Meteor. Soc. Japan*, **44**, 25–43, [https://doi.org/10.2151/jmsj1965.44.1\\_25](https://doi.org/10.2151/jmsj1965.44.1_25).

Mitchell, J. L., and G. K. Vallis, 2010: The transition to superrotation in terrestrial atmospheres. *J. Geophys. Res.*, **115**, E12008, <https://doi.org/10.1029/2010JE003587>.

Polvani, L. M., and J. Esler, 2007: Transport and mixing of chemical air masses in idealized baroclinic life cycles. *J. Geophys. Res.*, **112**, D23102, <https://doi.org/10.1029/2007JD008555>.

Potter, S. F., G. K. Vallis, and J. L. Michell, 2014: Spontaneous superrotation and the role of Kelvin waves in an idealized dry

- GCM. *J. Atmos. Sci.*, **71**, 596–614, <https://doi.org/10.1175/JAS-D-13-0150.1>.
- Ripa, P., 1983: General stability conditions for zonal flows in a one-layer model on the  $\beta$ -plane or the sphere. *J. Fluid Mech.*, **126**, 463–489, <https://doi.org/10.1017/S0022112083000270>.
- Sakai, S., 1989: Rossby-Kelvin instability: A new type of ageostrophic instability caused by a resonance between Rossby waves and gravity waves. *J. Fluid Mech.*, **202**, 149–176, <https://doi.org/10.1017/S0022112089001138>.
- Saravanan, R., 1993: Equatorial superrotation and maintenance of the general circulation in two-level models. *J. Atmos. Sci.*, **50**, 1211–1227, [https://doi.org/10.1175/1520-0469\(1993\)050<1211:ESAMOT>2.0.CO;2](https://doi.org/10.1175/1520-0469(1993)050<1211:ESAMOT>2.0.CO;2).
- Sardeshmukh, P. D., and B. J. Hoskins, 1988: The generation of global rotational flow by steady idealized tropical divergence. *J. Atmos. Sci.*, **45**, 1228–1251, [https://doi.org/10.1175/1520-0469\(1988\)045<1228:TGOGRF>2.0.CO;2](https://doi.org/10.1175/1520-0469(1988)045<1228:TGOGRF>2.0.CO;2).
- Scott, R., and L. M. Polvani, 2008: Equatorial superrotation in shallow atmospheres. *Geophys. Res. Lett.*, **35**, L24202, <https://doi.org/10.1029/2008GL036060>.
- Shell, K. M., and I. M. Held, 2004: Abrupt transition to strong superrotation in an axisymmetric model of the upper troposphere. *J. Atmos. Sci.*, **61**, 2928–2935, <https://doi.org/10.1175/JAS-3312.1>.
- Showman, A. P., and L. M. Polvani, 2010: The Matsuno-Gill model and equatorial superrotation. *Geophys. Res. Lett.*, **37**, L18811, <https://doi.org/10.1029/2010GL044343>.
- , and —, 2011: Equatorial superrotation on tidally locked exoplanets. *Astrophys. J.*, **738**, 71, <https://doi.org/10.1088/0004-637X/738/1/71>.
- Suarez, M. J., and D. G. Duffy, 1992: Terrestrial superrotation: A bifurcation of the general circulation. *J. Atmos. Sci.*, **49**, 1541–1554, [https://doi.org/10.1175/1520-0469\(1992\)049<1541:TSABOT>2.0.CO;2](https://doi.org/10.1175/1520-0469(1992)049<1541:TSABOT>2.0.CO;2).
- Suhas, D., J. Sukhatme, and J. M. Monteiro, 2017: Tropical vorticity forcing and superrotation in the spherical shallow-water equations. *Quart. J. Roy. Meteor. Soc.*, **143**, 957–965, <https://doi.org/10.1002/qj.2979>.
- Vallis, G. K., 2006: *Atmospheric and Oceanic Fluid Dynamics*. Cambridge University Press, 745 pp.
- Vanneste, J., and I. Yavneh, 2007: Unbalanced instabilities of rapidly rotating stratified shear flows. *J. Fluid Mech.*, **584**, 373–396, <https://doi.org/10.1017/S002211200700643X>.
- Wang, P., and J. L. Mitchell, 2014: Planetary ageostrophic instability leads to superrotation. *Geophys. Res. Lett.*, **41**, 4118–4126, <https://doi.org/10.1002/2014GL060345>.
- Williams, G. P., 2003: Barotropic instability and equatorial superrotation. *J. Atmos. Sci.*, **60**, 2136–2152, [https://doi.org/10.1175/1520-0469\(2003\)060<2136:BIAES>2.0.CO;2](https://doi.org/10.1175/1520-0469(2003)060<2136:BIAES>2.0.CO;2).
- Winter, T., and G. Schmitz, 1998: On divergent barotropic and inertial instability in zonal-mean flow profiles. *J. Atmos. Sci.*, **55**, 758–776, [https://doi.org/10.1175/1520-0469\(1998\)055<0758:ODBAII>2.0.CO;2](https://doi.org/10.1175/1520-0469(1998)055<0758:ODBAII>2.0.CO;2).